EPJ Web of Conferences **126**, 02001 (2016) DOI: 10.1051/epjconf/201612602001
*ICNFP 2015*

# Flavour physics at LHCb

B. Adeva[1,a], on behalf of the LHCb Collaboration.

[1] *University of Santiago de Compostela, Spain*

**Abstract.** Some selected results of the LHCb experiment, running at the LHC with $pp$ collisions at 7 TeV and 8 TeV, are reported here, after operation with a total integrated luminosity of 3.0 fb$^{-1}$ (Run 1). We focus on the most recent analyses on flavour physics, that include measurements of the CKM invariant phases $\gamma$ and $\beta$, precision determination of the quark coupling strength $V_{ub}$, observation of the very rare decays $B^0_{(s)} \to \mu^+\mu^-$, search for new physics in the anomalous branching ratio of $B \to D^*\tau\bar{\nu}$, and precision angular analysis of the rare decays $B^0 \to K^{*0}\mu^+\mu^-$ and $B^0_s \to \phi\mu^+\mu^-$. Detailed comparisons are performed in all cases with the predictions of the Standard Model, and a few interesting tensions are observed.

## 1 The LHCb experiment

The LHCb detector [1, 2] is one of the four major detectors at the Large Hadron Collider. It is instrumented in a cone arround the proton beam axis, covering the angles between 10 and 250 mrad, where most $b$ hadron decays produced in proton-proton collisions occur. The detector includes a high-precision tracking system with a dipole magnet, providing a measurement of momentum and impact parameter (IP), defined for charged particles as the minimum distance of a track to a primary $pp$ interaction vertex (PV). Different types of charged particles are distinguished using information from two ring-imaging Cherenkov detectors, a calorimeter and a muon system. Simulated samples of specific signal and background decay modes of $b$ hadrons are used at many stages throughout the analysis. These simulated events model the experimental conditions in full detail, including the $pp$ collision, the decay of the particles, and the response of the detector [3–5].

Candidates of the different signal modes reported in this article are required to pass a trigger system [6] which reduces in real time the rate of recorded collisions from the readout clock of the LHC to approximately 4 KHz. For muon channels, a muon is typically selected with $p_T > 1.48$ GeV/c in the $\sqrt{s} = 7$ TeV collision data ($p_T > 1.76$ GeV/c in the 8 TeV data), and at least one of the final-state particles is required to have both $p_T > 0.8$ GeV/c and impact parameter larger than 100 $\mu$m with respect to all of the PVs in the event. For hadron channels, a multivariate algorithm is used for the identification of secondary vertices consistent with the decay of a $b$ hadron [7]. In all cases, the tracks of two or more of the final-state particles are required to form a vertex that is significantly displaced from the PVs.

[a] e-mail: Bernardo.Adeva@usc.es

## 2 Measurement of the $\gamma$ CKM phase

In the Standard Model (SM), the Flavor Changing Charged Current processes of quarks are described by a unitary complex-valued Cabibbo-Kobayashi-Maskawa (CKM) mixing matrix [8], whose elements $V_{ij}$, with $i = u, c, t$ and $j = d, s, b$, quantify the relative $i \leftrightarrow j$ coupling strength. This matrix originates from the misalignment between up and down type quark couplings to the Higgs boson, and being unitary, it has only one independent phase.

Every CP violation phenomenon (in the quark sector) should be related, in the SM, to this unique phase. However, up to four measurable phases can be formed from combinations of the type $V_{\alpha i}V^*_{\alpha j}V_{\beta j}V^*_{\beta i}$, and it is important to measure all of them because loop-level contributions from additional high-mass particles beyond the SM, may alter the unitarity relationships they must fulfil.

The measurement of the phase $\beta = \arg\left[-V_{cd}V^*_{cb}/(V_{td}V^*_{tb})\right]$, that provided the first evidence for CP-violation in the $b$-quark sector [9], is a historical example. A new competitive measurement of this parameter has been provided this year by the LHCb experiment, which is reported in the next section. Yet another sensitive test of the SM comes from measurements of the phase $\beta_s = \arg\left[-V_{ts}V^*_{tb}/(V_{cs}V^*_{cb})\right]$, only accessible from $B^0_s$ meson decays, which is predicted to be very small in the SM. LHCb has initiated a series of measurements of this parameter using different channels, which we are not discussing here [10]. Within the precision attained so far, these measurements appear to confirm the SM prediction.

In order to disentangle the nature of new physics contributions from quantum loops, in case a significant deviation from unitarity is found, it is particularly important to have a CP-observable that only receives contributions from tree-level diagrams, and can therefore be used as a test-bench for the SM. This is precisely the case with the phase $\gamma = \arg[-V_{ud}V^*_{ub}/(V_{cd}V^*_{cb})]$ [11], the least well-measured to date of those in the unitarity triangle $V_{ud}V^*_{ub} + V_{cd}V^*_{cb} + V_{td}V^*_{tb} = 0$.

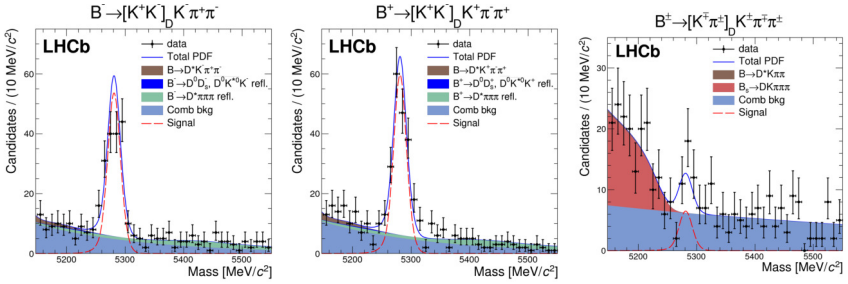


**Figure 1.** Mass distributions of $B^- \to DX_s^-$ candidates using GLW selections , for $B^- \to [K^+K^-]_D X_s^-$ (left), $B^- \to [K^+K^-]_D X_s^+$ (center), and the suppressed ADS mode, $B^\pm \to [K^\mp\pi^\pm]_D K^\pm\pi^\mp\pi^\mp$ , sum of $B^+$ and $B^-$ (right).

The phase $\gamma$ can be probed by studying the interference between $b \to u$ and $b \to c$ transitions, such as the interference between $B^- \to D^0K^-$ and $B^- \to \bar{D}^0K^-$, when states accessible to both $D^0$ and $\bar{D}^0$ mesons are selected. A number of methods have been discussed in the literature, and are often grouped into three categories, depending on the D decay mode: (i) CP eigenstates, such as $D \to K^+K^-$ and $D \to \pi^+\pi^-$ (GLW) [12]; (ii) flavor-specific final states, such as the Cabibbo-favored and double Cabibbo suppressed $D \to K^\pm\pi^\mp$ decays (ADS) [13]; and (iii) multi-body self-conjugate final states, such as $D \to K^0_s\pi^+\pi^-$ (GGSZ) [14].

Measurements of $\gamma$ have been performed from averages over several decay modes from individual experiments, and the current experimental status is $\gamma = (73^{+9}_{-10})^\circ$ by the LHCb collaboration [16],

$\gamma = (73^{+17}_{-16})^\circ$ by the BaBar collaboration [17], and $\gamma = (68^{+15}_{-14})^\circ$ by the Belle collaboration [18]. The overall precision on $\gamma$ from a global fit is about 7° [19]. In order to improve the overall precision, it is important to study a wide range of final states. It has been suggested that other multi-body final states of the recoiling strange quark system could be useful [15], due to their larger branching fractions, and potentially larger interference contribution.

LHCb has performed the first ADS and GLW analyses of the decay $B^- \to DX_s^-$, where the $D$ meson is observed through its decay to $K^\pm\pi^\mp$, $K^+K^-$ and $\pi^+\pi^-$, and a multibody final state $X_s^- \equiv K^-\pi^+\pi^-$ is defined for the recoil system [20]. Some invariant mass spectra for the $B^- \to DX_s^-$ ADS and GLW signal modes are shown in Fig.1. The analysis uses an integrated luminosity of 3.0 fb$^{-1}$ and includes the modes $B^- \to DX_d^-$, with lower sensitivity to $\gamma$, for normalization purposes. Significant signals are observed in the CP modes for both the favored and the suppressed $B^-$ decays, and first evidence is seen for the ADS DCS $B^- \to D[K^+\pi^-]_D K^-\pi^+\pi^-$ decay. A fit for $\gamma$ is performed, from which $\gamma = (74^{+20}_{-22})^\circ$ is found with only $B^- \to DX_s^-$ modes. Values of $\gamma$ below about 25° and larger than approximately 165° are not excluded by these modes, but are excluded when other modes are considered [16]. The sensitivity to $\gamma$ from this analysis makes it a promising channel for future studies.

LHCb has also explored additional multibody final states leading to possible improvement of the global precision on the $\gamma$ parameter, and performed a measurement of CP observables from $B^\pm \to Dh^\pm$ decays, where D mesons are reconstructed in the ADS channel $D \to K^\mp\pi^\pm\pi^0$ and the quasi-GLW modes $D \to \pi^+\pi^-\pi^0$ and $D \to K^+K^-\pi^0$ [21]. In such cases, the interference effects that are sensitive to $\gamma$ vary over the phase space of the D decay, due to the role of strongly-decaying intermediate resonances, and the integration over the phase space in general dilutes the net sensitivity. For multi body ADS/GLW modes the dilution factor can be measured with $D\bar{D}$ pairs coherently produced at the $\psi(3770)$ resonance [22]. Recent measurements of this type [23] indicate that the dilution effects in $D \to K^\mp\pi^\pm\pi^0$ and $D \to \pi^+\pi^-\pi^0$ are rather small, making these decays particularly suitable for an inclusive analysis. In particular the latter is very close to being a CP-even eigenstate, and the interference terms suffer very little dilution.

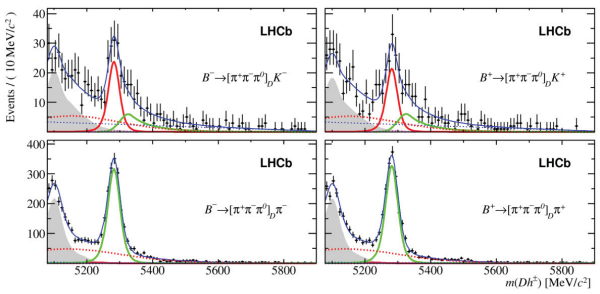


**Figure 2.** Invariant mass distributions of selected $B^\mp \to [\pi^+\pi^-\pi^0]_D h^\mp$ candidates, separated by B hadron charge. $B^\mp \to DK^\mp$ signal events are in the upper plots and $B^\mp \to D\pi^\mp$ in the lower plots.The red curve represents $DK^\mp$ events and the green curve represents $D\pi^\mp$ events. The grey shape indicates partially reconstructed $B^\mp$ decays and the dotted red curve indicates wrongly reconstructed D decays. The blue line represents the total PDF

As it is described in Ref. [21], twelve observables are measured by LHCb in total, including CP-asymmetries and amplitude ratios between Cabibbo favored and suppressed modes, for the above-mentioned ADS and quasi-GLW modes. Two-dimensional scans are performed for $\gamma$ vs. $r_B$ and $\gamma$ vs. $\delta_B$, where the hadronic amplitude ratio $r_B$ and the phase difference $\delta_B$ are defined as: $A(B^- \to \bar{D}^0K^-)/A(B^- \to D^0K^-) = r_B e^{i(\delta_B-\gamma)}$. The results are compatible with the values obtained from a global analysis of other LHCb measurements sensitive to $\gamma$ at tree level (also sensitive to $r_B$ and $\delta_B$) [16]. No evidence of CP violation is seen with the current experimental precision. First evidence is obtained for the mode $B^\mp \to [K^+K^-\pi^0]_D K^\mp$, and the channels $B^\mp \to [\pi^\mp K^\pm\pi^0]_D\pi^\mp$ $B^\mp \to [K^+K^-\pi^0]_D\pi^\mp$ have been observed for the first time. Some particular invariant mass spectra are

shown in Fig.2, separated by the charge of the $B^{\mp}$ candidate, as an indication of the signal significance for CP violating observables.

When analysed in the context of the underlying physics parameters, the results exhibit good consistency with other LHCb measurements, and they will be valuable in improving knowledge of $\gamma$ in the unitarity triangle $V_{ud}V_{ub}^{*} + V_{cd}V_{cb}^{*} + V_{td}V_{tb}^{*} = 0$, when combined with results from $B^{\mp} \to DK^{\mp}$ measurements using other D decay channels.

## 3 New precision measurement of the $\beta$ CKM phase

The violation of CP symmetry in processes involving $B$ mesons was first observed in the "golden mode" $B^0 \to J/\psi K_s^0$ by the BaBar and Belle experiments at the asymmetric $e^+e^-$ colliders PEP-II and KEKB. Since then, measurements of CP violation in this decay mode have reached a precision at the level of $10^{-2}$ [24]. LHCb has performed a new competitive measurement obtained at a hadron collider [25], where a reduced flavor tagging capability, as compared to B-factories, is compensated by a higher $b$ hadron cross-section, with the integrated luminosity of 3.0 fb$^{-1}$ from Run 1.

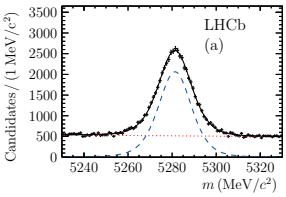


**Figure 3.** The distribution of the reconstructed mass of tagged $B^0 \to J/\psi K_s^0$ candidates is shown. The solid black line shows the fit projection, while the dashed (dotted) line shows the projection for the signal (background) components only.

As the $J/\psi K_s^0$ final state is common to both $B^0$ and $\bar{B}^0$ meson decays, the interference between the amplitudes for the direct decay and for the decay after $B^0 - \bar{B}^0$ oscillation results in a decay-time dependent CP asymmetry as follows

$$A(t) \equiv \frac{\Gamma(\bar{B}^0(t) \to J/\psi K_s^0) - \Gamma(B^0(t) \to J/\psi K_s^0)}{\Gamma(\bar{B}^0(t) \to J/\psi K_s^0) + \Gamma(B^0(t) \to J/\psi K_s^0)} = \frac{S\,\sin(\Delta m t) - C\cos(\Delta m t)}{\cosh(\frac{\Delta\Gamma t}{2}) + A_{\Delta\Gamma}\sinh(\frac{\Delta\Gamma t}{2})}$$

where $B^0(t)$ and $\bar{B}^0(t)$ indicate the flavor of the $B$ meson at production, while $t$ indicates the decay time. The parameters $\Delta m$ and $\Delta\Gamma$ are the mass and decay width differences between the heavy and light mass eigenstates of the $B^0 - \bar{B}^0$ system, and $S$, $C$ and $A_{\Delta\Gamma}$ are CP observables. As $\Delta\Gamma$ is negligible for the $B^0 - \bar{B}^0$ system, the time dependent asymmetry simplifies to $A(t) = S\,\sin(\Delta m t) - C\cos(\Delta m t)$. The $B^0 \to J/\psi K_s^0$ decay is dominated by a $\bar{b} \to c\bar{c}\bar{s}$ transition, and CP violation in the decay is expected to be negligible at the current level of experimental precision, giving $C \approx 0$, which allows to identify $S$ with $\sin(2\beta)$.

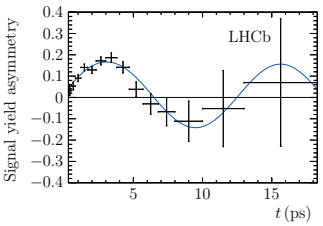


**Figure 4.** The time-dependent signal-yield asymmetry $(N_{\bar{B}^0} - N_{B^0})/(N_{\bar{B}^0} + N_{B^0})$ is shown. Here $N_{B^0}$ ( $N_{\bar{B}^0}$) is the number of $B^0 \to J/\psi K_s^0$ decays with a $B^0$ ($\bar{B}^0$) flavor tag. The solid curve is the projection of the signal PDF.

Compared to previous LHCb analysis, the effective tagging efficiency $\epsilon_{eff}$ has increased from 2.38% to 3.02%, mainly due to the inclusion of a same side pion tagger algorithm. The mass spectrum

of the selected candidates is shown in Fig. 3, and the measured decay-time dependent signal-yield asymmetry is shown in Fig. 4.

The CP observables $S$ and $C$ are measured to be

$$\begin{aligned} \mathrm{S} &= 0.731 \pm 0.035\ (\mathrm{stat}) \pm 0.020\ (\mathrm{syst}) \\ \mathrm{C} &= -0.038 \pm 0.032\ (\mathrm{stat}) \pm 0.005\ (\mathrm{syst}) \end{aligned}$$

with a statistical correlation $\rho(S, C) = 0.483$. When $C$ is fixed to zero the measurement yields $S = \sin(2\beta) = 0.746 \pm 0.030$ $(stat)$. This result represents the most precise time-dependent CP violation measurement at a hadron collider to date. Furthermore, it has a similar precision to, and is in good agreement with, previous measurements performed at the Belle and BaBar experiments at the KEKB and PEP-II colliders [24]. This result is in excellent agreement with expectations from other measurements and improves the consistency of the CKM sector of the Standard Model. Other measurements that constraint this angle of the unitarity triangle predict $\sin(2\beta)$ as $0.771^{+0.017}_{-0.041}$ [26].

## 4 Precision determination of the coupling strength $|V_{ub}|$

The $V_{ub}$ matrix element governs the most sensitive misalignment in the couplings between the up and down type quark flavors to the Higgs boson. Its apparent proportionality to the third power of $\lambda$ (sine of the Cabibbo angle) remains unexplained, and it best quantifies the minimal flavor violation structure of the Standard Model. A precision measurement of the magnitude of $V_{ub}$ is naturally achieved via the semileptonic quark-level transition $b \to u l^- \bar{\nu}_l$, which minimizes hadronic uncertainties. There are two complementary methods to perform such measurement. The simplest is to measure the branching fraction of a specific (exclusive) decay such as $\bar{B}^0 \to \pi^+ l^- \bar{\nu}$ or $B^- \to \pi^0 l^- \bar{\nu}$, where the influence of the strong interaction in the decay, encompassed by the $\bar{B}^0 \to \pi^+$ form factor, is predicted by lattice QCD (LQCD) [28] or QCD sum rules [29]. The world average from Ref. [30] is $V_{ub} = (3.28 \pm 0.29) \times 10^{-3}$, where the most precise inputs come from the Babar [31] and Belle [32] experiments. The uncertainty is dominated by the LQCD calculations, recently updated [33]. The alternative method is measure the differential decay rate in an inclusive way over all possible $B$ meson decays containing the $b \to u l^- \bar{\nu}_l$ quark level transition. This results in $V_{ub} = (4.41^{+0.15}_{-0.17}) \times 10^{-3}$ [34], where the second uncertainty comes from theoretical calculations. The above results are summarized in Fig.5 (left).

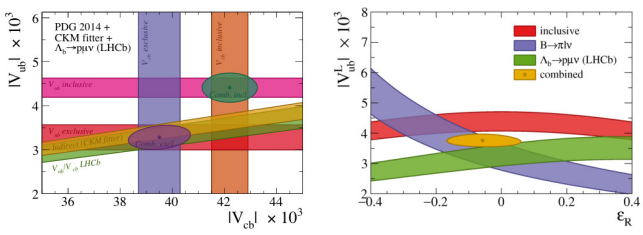


**Figure 5.** Summary of the exclusive and inclusive measurements indicated in the text (left) and experimental constraints on left-handed coupling, $V^L_{ub}$ and the fractional right-handed (RH) coupling $\epsilon_R$. While the overlap of the 68% CL bands for the inclusive and exclusive world averages suggested a RH coupling of significant magnitude, the inclusion of the LHCb measurement does not support this.

The discrepancy between the exclusive and the inclusive $V_{ub}$ determinations has a significance of approximately $3\sigma$ and has been a long standing puzzle in flavor physics. Several explanations have been proposed, such as the presence of a right-handed $(V + A)$ W coupling [35].

LHCb has performed a measurement of the ratio of branching fractions of the $\Lambda^0_b$ into $p\mu^-\bar{\nu}_\mu$ and $\Lambda^+_c\mu^-\bar{\nu}_\mu$ final states [27]. This has been done using $pp$ collisions from the LHC, corresponding to 2.0 $fb^{-1}$ of integrated luminosity at 8 TeV. The $b \to u$ transition $\Lambda^0_b \to p\mu^-\bar{\nu}_\mu$ could not be considered before at B-factories, but becomes feasible at the LHC.

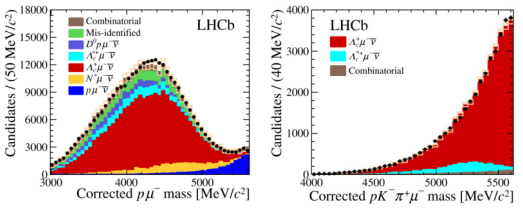


**Figure 6.** Fits are made for $\Lambda_b^0 \to p\mu^-\bar{\nu}$ (left) and $\Lambda_b^0 \to \Lambda_c^+(pK^-\pi^+)\mu^-\bar{\nu}$ (right) candidates. Data are represented by the black points, and the open boxes represent the statistical uncertainties from the finite size of the simulation samples used to model the mass shapes. There are no data above the nominal $\Lambda_b^0$ mass due to the removal of unphysical $q^2$ solutions.

To facilitate $\Lambda_b^0$ reconstruction at a hadron collider, LHCb introduces a corrected mass $M_{corr} = \sqrt{m_{h\mu}^2 + p_\perp{}^2} + p_\perp{}^2$ where $h$ represents either the proton or the $\Lambda_c^+$ candidate, $m_{h\mu}$ is the visible mass of the $h\mu$ pair, and $p_\perp$ is the momentum of the $h\mu$ pair transverse to the $\Lambda_b^0$ flight direction.The recoil squared mass $q^2(\mu\nu)$ can be determined from the above direction, up to a two-fold ambiguity. For kinematic reasons in the experiment, it is restricted to high values, precisely where the precision on the form factors is best. Secondary vertex isolation criteria are used, and from a detailed comparison between the $M_{corr}$ spectra shown in Fig. 6, a measurement of the ratio of branching ratios is achieved:

$$\frac{\mathcal{B}(\Lambda_b^0 \to p\mu^-\bar{\nu}_\mu)_{q^2>15GeV/c^2}}{\mathcal{B}(\Lambda_b^0 \to \Lambda_c^+\mu^-\bar{\nu}_\mu)_{q^2>7GeV/c^2}} = (1.00 \pm 0.04 \pm 0.08) \times 10^{-2}$$

using the form factor information from [36] for the restricted $q^2$ regions, the measurement $|V_{ub}|/|V_{cb}| = 0.083 \pm 0.004 \pm 0.004$ is obtained, where the second uncertainty arises from the uncertainty in the LQCD prediction. When the exclusive world average is used for $|V_{cb}|$ [34], the measurement is obtained

$$|V_{ub}| = (3.27 \pm 0.15 \pm 0.17 \pm 0.06) \times 10^{-3}$$

where the uncertainties indicate experimental, LQCD prediction and normalization to $V_{cb}$. The determination of $|V_{ub}|$ from the ratio of branching ratios depends on the size of a possible right-handed coupling [35], according to an effective Lagangian of the type

$$\mathcal{L}_{eff} = -\frac{4G_F}{\sqrt{2}} V_{ub}^L \left(\bar{u}\gamma_\mu P_L b + \epsilon_R \bar{u}\gamma_\mu P_R b\right)(\bar{\nu}\gamma^\mu P_L l) + h.c.$$

with $P_{R,L} = (1 \pm \gamma^5)/2$. The sensitivity can be appreciated in Fig. 5 (right) which shows the experimental constraints on the left-handed coupling $|V_{ub}^L|$ and the fractional right-handed coupling added to the SM, $\epsilon_R$ for different measurements. Unlike the case for the pion in $\bar{B}^0 \to \pi^+ l^-\bar{\nu}$ and $B^- \to \pi^0 l^-\bar{\nu}$ decays, the spin of the proton is non-zero, allowing an axial-vector current, which gives a different sensitivity to $\epsilon_R$. The overlap of the bands from the previous measurements suggested a significant right-handed coupling, but the inclusion of the LHCb $|V_{ub}|$ measurement does not support that assumption.

In summary, the most precise measurement to date of $|V_{ub}|$ is reported using the exclusive decay mode $\Lambda_b^0 \to p\mu^-\bar{\nu}_\mu$. The measurement is in agreement with the exclusively measured world average [30], but disagrees with the inclusive measurement [34] at a significance level of $3.5\sigma$. The measurement will have an important impact on the global fits to the parameters of the CKM matrix.

## 5 Observation of the very rare decays $B^0_{(s)} \to \mu^+\mu^-$

The decay of the $B^0_s$ meson into dimuons is suppressed strongly, to the level $10^{-9} - 10^{-10}$. It represents a powerful probe in testing new physics effects, because the suppression originates from essential features of the heavy particle spectrum of the SM, namely: the GIM mechanism, helicity suppression and the fact that the SM contributions involve an off-diagonal element of the CKM matrix.

Since these features are of course not generally respected by generic extensions of the SM, the above decay has been searched for many years at most generations of accelerators. The Feynman diagrams are shown in Fig. 7, illustrating the suppression in the SM and the sensitivity to Supersymmetry models.

The first evidence for the $B^0_s \to \mu^+\mu^-$ decay was presented by the LHCb collaboration in 2012 [47]. The LHCb and CMS experiments have presented a joint analysis [48], in order to fully exploit the statistical power of the LHC data, and take into account the correlation between the physical quantities in common to the two analyses. The data correspond to total integrated luminosities of 25.0 fb$^{-1}$ and 3.0 fb$^{-1}$ for the CMS and LHCb experiments, respectively. This is equivalent to a total of approximately $10^{12} B^0_s$ and $B^0$ mesons produced in both experiments together, determined from the number of expected events assuming the SM branching fractions.

The branching fractions of these two decays, accounting for higher order electromagnetic and strong interaction effects, are reliably calculated in the SM. The untagged time-integrated SM predictions are $\mathcal{B}(B^0_s \to \mu^+\mu^-)_{SM} = (3.66 \pm 0.23) \times 10^{-9}$ and $\mathcal{B}(B^0 \to \mu^+\mu^-)_{SM} = (1.06 \pm 0.09) \times 10^{-10}$ [37], which use the latest lattice QCD results to compute $B^0_s$ and $B^0$ meson decay constants [38].

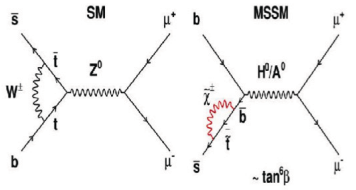


**Figure 7.** Some Feynman diagrams for the $B^0_s \to \mu^+\mu^-$ decay in (a) the SM and (b) Minimal Supersymmetric model.

Many theories that seek to go beyond the SM (BSM) include new phenomena and particles [39], such as in the diagram shown in Fig. 8(b), that can considerably modify the SM branching fractions. In particular, theories with additional Higgs bosons [40] predict possible enhancements of the branching fractions. A significant deviation of either of the two measurements from the SM predictions would give insight on how the SM should be extended. Alternatively, a measurement compatible with the SM could provide strong constraints on BSM theories.

The ratio of the branching fractions of the two decay modes additionally provides powerful discrimination among BSM theories [41]. In the SM it is predicted to be $\mathcal{B}(B^0 \to \mu^+\mu^-)_{SM} / \mathcal{B}(B^0_s \to \mu^+\mu^-)_{SM} = 0.0295^{+0.0028}_{-0.0025}$ [44], [45], [46]. Notably, BSM theories with the property of minimal flavor violation [42] predict the same value as the SM for this ratio.

The two experiments measure at different angular regions with respect to the LHC beams, according to their different design purposes. Their dimuon mass resolution are also different, namely $\approx 25$ MeV/$c^2$ for LHCb, and ranging from 32-76 MeV/$c^2$, depending on the pseudorapidity of the two tracks for CMS. The separation between genuine $B^0_s \to \mu^+\mu^-$ decays and random combinations of two muons, most often from semi-leptonic decays of two different $b$ hadrons, is achieved by means of boosted decision trees (BDTs) [43]. Each experiment selected the best set of discriminating variables in their respective BDT. One example is the decay length with respect to the PV. Having lifetimes of about 1.5 ps, $B^0_{(s)}$ mesons travel up to a few centimetres before they decay, with momenta between a few GeV/c and 100 GeV/c at the LHC. Candidates were categorized according to the value of the

relevant BDT discriminant, to whether they were detected in CMS or LHCb, and to the kinematical configuration of both muons, in the case of CMS. 20 different categories were so defined, as described in Ref. [48].

A single dimuon mass distribution, extended over all categories, is shown in Fig. 8. Event candidates are weighted according to their values of $S/(S+B)$, where $S$ is the expected number of $B_s^0$ signals and $B$ the number of background events under the $B_s^0$ peak in each category.

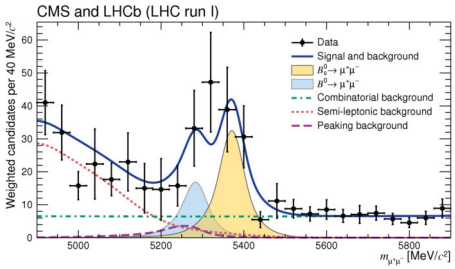


**Figure 8.** Weighted distribution of the dimuon invariant mass $m_{\mu^+\mu^-}$ for all categories defined within the CMS and LHCb experiments. Superimposed on the black data points are the combined fit (solid blue line) and its components: the $B_s^0$ (yellow shaded area) and $B^0$ (light blue shaded area) signal components, the combinatorial background (dashed-dotted green line); the sum of the semileptonic backgrounds (dotted salmon line); and the peaking backgrounds (dashed violet line).

Likelihood contours for $\mathcal{B}(B_s^0 \to \mu^+\mu^-)$ versus $\mathcal{B}(B^0 \to \mu^+\mu^-)$ are shown in Fig. 8. One-dimensional likelihood scans for both decay modes are displayed in the same figure. A combined fit leads to the measurements $\mathcal{B}(B_s^0 \to \mu^+\mu^-) = 2.8^{+0.7}_{-0.6} \times 10^{-9}$ and $\mathcal{B}(B^0 \to \mu^+\mu^-) = 3.9^{+1.6}_{-1.4} \times 10^{-10}$, where the uncertainties include both statistic and systematic sources. The statistical significance is computed to be $6.2\sigma$ for the $B_s^0 \to \mu^+\mu^-$ mode and $3.0\sigma$ for the $B^0 \to \mu^+\mu^-$ mode (we report the significance obtained with the FC method) .

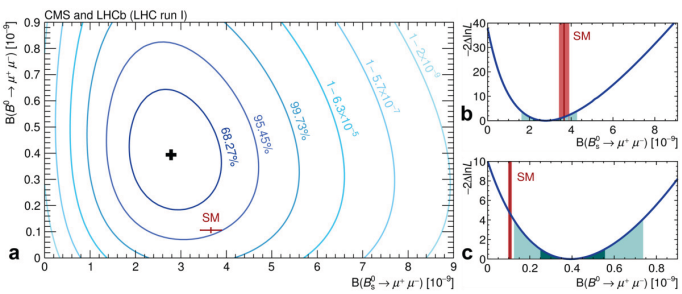


**Figure 9.** Likelihood contours in the $\mathcal{B}(B_s^0 \to \mu^+\mu^-)$ versus $\mathcal{B}(B^0 \to \mu^+\mu^-)$ plane. The (black) cross in (a) marks the best-fit central value. The SM expectation and its uncertainty is shown in the (red) marker. Each contour encloses a region corresponding to the reported confidence level. Variations of the test statistic -2lnL are also shown for $\mathcal{B}(B_s^0 \to \mu^+\mu^-)$ (b) and $\mathcal{B}(B^0 \to \mu^+\mu^-)$ (c). The dark and light (cyan) areas define the $\pm 1\sigma$ and $\pm 2\sigma$ confidence intervals, respectively. The SM prediction and its uncertainty is denoted with the vertical (red) band.

A fit for the ratios of the branching fractions relative to their SM predictions yields $\mathcal{S}^{B_s^0}_{SM} = 0.76^{+0.20}_{-0.18}$ and $\mathcal{S}^{B^0}_{SM} = 3.7^{+1.6}_{-1.4}$. The ratio of branching ratios themselves yields $\mathcal{R} = 0.14^{+0.08}_{-0.06}$ which is compatible with the SM at the $2.3\sigma$ level.

The combined analysis of the data from CMS and LHCb establishes conclusively the existence of the $B_s^0 \to \mu^+\mu^-$ decay and produces a $3\sigma$ evidence for the $B^0 \to \mu^+\mu^-$ decay. For $B_s^0$, this concludes a search that started more than three decades ago. A phase of even higher sensitivity and precision measurements is initiated for both decays.

## 6 Anomalous branching fraction of $B \to D^*\tau\bar{\nu}$

Lepton universality, which is preserved within the Standard Model, requires equality of couplings between gauge bosons and the three families of leptons. Hints for lepton nonuniversal effects in

$B^+ \to K^+e^+e^-$ and $B^+ \to K^+\mu^+\mu^-$ decays have been seen [50] , but no definitive observation of a deviation has yet been made. However, a large class of models that extend the SM contain additional interactions involving enhanced couplings to the third generation that would violate the above principle. Semileptonic decays of $b$ hadrons to third generation leptons provide a sensitive probe for such effects. In particular, the presence of additional charged Higgs bosons, which are often required in these models, can have a significant effect on the rate of the semitauonic decay $\bar{B}^0 \to D^{*+}\tau^-\bar{\nu}_\tau$ [51].

Semitauonic decays have been observed by BaBar and Belle collaborations [52],[56]. Recently BaBar reported updated measurements [55],[56] of the ratios of branching fractions, $\mathcal{R}(D^*) \equiv \mathcal{B}(\bar{B}^0 \to D^{*+}\tau^-\bar{\nu}_\tau)/\mathcal{B}(\bar{B}^0 \to D^{*+}\mu^-\bar{\nu}_\tau)$ and $\mathcal{R}(D) \equiv \mathcal{B}(\bar{B}^0 \to D^{+}\tau^-\bar{\nu}_\tau)/\mathcal{B}(\bar{B}^0 \to D^{+}\mu^-\bar{\nu}_\tau)$, which show deviations of $2.7\sigma$ and $2.0\sigma$, respectively, from the SM predictions [57],[58]. These ratios have been calculated with high precision, owing to the cancelation of most of the uncertainties associated with the strong interaction in the $B$ to $D^{(*)}$ transition. Within the SM they differ because of phase-space effects due to the differing charged lepton masses.

LHCb has achieved a new measurement of $\mathcal{R}(D^*)$ using hadron collisions at the LHC with an integrated luminosity of 1.0 fb$^{-1}$ and 2.0 fb$^{-1}$ collected at $pp$ center-of-mass energies of 7 TeV and 8 TeV, respectively [49]. The $\bar{B}^0 \to D^{*+}\tau^-\bar{\nu}_\tau$ decay with $\tau^- \to \mu^-\bar{\nu}_\mu\nu_\tau$ (the signal channel) and the $\bar{B}^0 \to D^{*+}\mu^-\bar{\nu}_\tau$ decay (normalization channel) produce identical visible final-state topologies; consequently both are selected by a common reconstruction procedure. The selection identifies semileptonic $\bar{B}^0$ decay candidates containing a muon candidate and a $D^{*+}$ candidate through the decay chain $D^{*+} \to D^0(\to K^-\pi^+)\pi^+$. The selected sample contains contributions from the signal and the normalization channel, as well as several background processes from hadron collisions, which include partially reconstructed $B$ decays and candidates from combinations of unrelated particles from different $b$ hadron decays. The kinematic and topological properties of the various components are exploited to suppress the background contributions. The signal, the normalization component and the residual background are statistically disentangled with a multidimensional fit to the data, using template distributions derived from control samples, or from simulation validated against real data.

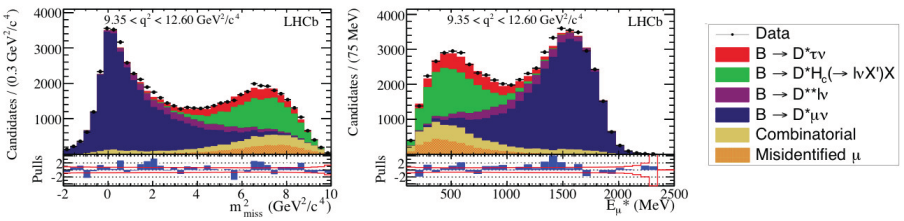


**Figure 10.** Distributions of $m^2_{miss}$ (left) and $E^*_\mu$ (right) of one of the four $q^2$ bins of the signal data used in the fit ($9.35<q^2<12.60$ GeV$^2$/c$^4$), overlaid with projections of the fit model with all normalization and shape parameters at their best-fit values. Below each pannel differences between the data and fit are shown, normalized by the Poisson uncertainty in the data. The bands give the $1\sigma$ template uncertainties.

The separation of the signal from the normalization channel, as well as from background processes, is achieved by exploiting the distinct kinematic distributions resulting from the $\mu$-$\tau$ mass difference and the presence of extra neutrinos from the decay $\tau^- \to \mu^-\bar{\nu}_\mu\nu_\tau$. The most discriminating kinematic variables, computed in the $B$ rest frame, are the following quantities: the muon energy $E^*_\mu$; the missing mass squared, defined as $m^2_{miss} = (p^\mu{}_B - p^\mu{}_D - p^\mu{}_\mu)^2$; and the squared four-momentum transfer to the lepton system, $q^2 = (p^\mu{}_B - p^\mu{}_D)^2$, where $P^\mu_B$, $P^\mu_D$, and $P^\mu_\mu$ are the four momenta of the $B$ meson, the $D^{*+}$ meson and the muon. The determination of the rest-frame variables requires knowl-

ege of the $B$ candidate momentum vector, which is estimated from the measured parameters of the reconstructed final-state particles. The $B$ momentum direction is determined from the unit vector to the $B$ decay vertex from the associated PV.

The results of the fit to the signal sample are shown in Fig. 10. Values of the $\bar{B}^0 \to D^{*+}\mu^-\bar{\nu}_\mu$ form factor parameters determined from the fit agree with the current world average values. The fit finds 363000 ± 1600 $\bar{B}^0 \to D^{*+}\mu^-\bar{\nu}_\mu$ decays in the signal sample and an uncorrected ratio of yields $N(\bar{B}^0 \to D^{*+}\tau^-\bar{\nu}_\tau)/N(\bar{B}^0 \to D^{*+}\mu^-\bar{\nu}_\mu) = (4.54 \pm 0.46) \times 10^{-2}$. Accounting for the $\tau^- \to \mu^-\bar{\nu}_\mu\nu_\tau$ branching fraction and the ratio of efficiencies results in $\mathcal{R} = 0.336 \pm 0.034$, where the uncertainty includes the statistical uncertainty, the uncertainty due to form factors, and the statistical uncertainty in the kinematic distributions used in the fit. The measured value is in good agreement with previous measurements by BABAR and Belle [52],[54] and is $2.1\sigma$ greater than the SM expectation of 0.252 ± 0.003 [57].

## 7 Angular analysis of $b \to s\mu^+\mu^-$ decays

The decay $B^0 \to K^{*0}(\to K^+\pi^-)\mu^+\mu^-$ is a $b \to s\mu^+\mu^-$ flavor-changing neutral current (FCNC) transition that has attracted a great deal of interest at B-factories and hadron machines, in recent years. In the Standard Model (SM) the decay is forbidden at tree level and, at lowest order, only occurs via electroweak penguin and box processes. In extensions of the SM, new, heavy particles can enter in competing processes and can significantly change the branching fraction of the decay and the angular distribution of the final state particles. In Fig. 11 some representative diagrams of either case are shown.

Angular observables are of particular interest, since theoretical predictions of such observables tend to be less affected by form-factor uncertainties in the $B^0 \to K^{*0}$ transition. Hereafter $K^{*0}$ is used to refer to the $K^{*0}(892)$.

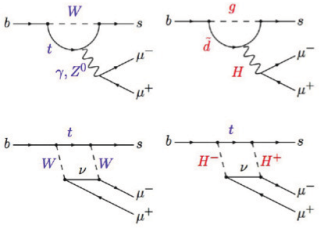


**Figure 11.** Some illustrating diagrams indicating the penguin loops and box contributions from the SM to $B^0 \to K^{*0}\mu^+\mu^-$ decay (left side ones), and contributions from new Higgs particles in physics beyond the SM (right side ones)

Based on 1.0 fb$^{-1}$, the LHCb collaboration published in 2013 an analysis of the $B^0 \to K^{*0}\mu^+\mu^-$ final state, and determined a set of angular observables that have reduced theoretical uncertainties and cannot be determined from the single angular projections [61]. The above analysis found a local deviation from the SM prediction, with a significance corresponding to $3.7\sigma$ in one observable, $P_5^{'}$. Possible interpretations of this discrepancy and the consistency of all of the measurements of $b \to s$ transitions have been widely discussed in recent literature [59]. LHCb has performed an updated analysis using the full LHCb Run 1 data sample [60], corresponding to an integrated luminosity of 3.0 fb$^{-1}$.

The final state of the decay $B^0 \to K^{*0}\mu^+\mu^-$ can be fully described by $q^2$, the invariant mass of the dimuon system squared, and three decay angles $\vec{\Omega} = (\cos\theta_l, \cos\theta_K, \phi)$, where $\theta_{l,K}$ are the helicity angles in the $K^{*0}$ and dimuon system, and $\phi$ describes the angle between the $\mu^+\mu^-$ plane and the $K^+\pi^-$ plane, defined in the $B^0$ rest frame. The differential decay rates of $\bar{B}^0 \to \bar{K}^{*0}\mu^+\mu^-$ and $B^0 \to K^{*0}\mu^+\mu^-$ are given by

$$\frac{d^4\Gamma[\bar{B}^0 \to \bar{K}^{*0}\mu^+\mu^-]}{dq^2 d\vec{\Omega}} = \frac{9}{32\pi}\sum_j I_j(q^2) f_j(\vec{\Omega}) \ , \quad \frac{d^4\bar{\Gamma}[B^0 \to K^{*0}\mu^+\mu^-]}{dq^2 d\vec{\Omega}} = \frac{9}{32\pi}\sum_j \bar{I}_j(q^2) f_j(\vec{\Omega})$$

where the terms $f_j(\vec{\Omega})$ arise from spherical harmonics and the $I_j(q^2)$ are eleven $q^2$ dependent angular observables. The $I_j(q^2)$ can be expressed as bilinear combinations of six complex decay amplitudes $\mathcal{A}^{L,R}_{0,\|,\perp}$, which correspond to different transversity states of the $K^{*0}$ and different (left- and right-handed) chiralities of the dimuon system. Following the notation in [65], CP-averaged observables can be defined as

$$S_j = \left(I_j + \bar{I}_j\right) \Big/ \left(\frac{d\Gamma}{dq^2} + \frac{d\bar{\Gamma}}{dq^2}\right)$$

If $q^2$ is sufficiently large ($q^2 \gtrsim 1$ GeV$^2$/c$^4$), the muons can be considered massless and the CP-averaged observables $S_1$ and $S_2$ obey the relations $S_{1s} = 3S_{2s}$, $S_{1c} = -S_{2c}$ and $\frac{3}{4}(2S_{1s} + S_{1c}) - \frac{1}{4}(2S_{2s} + S_{2c}) = 1$ (see for example Ref. [65]). These relationships reduce the number of observables from eleven to eight. The $S_{1c}$ observable is more commonly expressed in terms of the longitudinal polarization fraction of the $K^{*0}$,

$$F_{\rm L} = S_{1c} = \frac{|\mathcal{A}^L_0|^2 + |\mathcal{A}^R_0|^2}{|\mathcal{A}^L_0|^2 + |\mathcal{A}^R_0|^2 + |\mathcal{A}^L_\||^2 + |\mathcal{A}^R_\||^2 + |\mathcal{A}^L_\perp|^2 + |\mathcal{A}^R_\perp|^2}$$

It is also conventional to replace $S_{6s}$ by the forward-backward asymmetry of the dimuon system $A_{\rm FB}$, where $A_{\rm FB} = \frac{3}{4}S_{6s}$. Additional sets of observables, for which the leading form-factor uncertainties cancel, can be built from $F_{\rm L}$ and $S_3$ through $S_9$. Examples of such "optimized" observables include the transverse asymmetry $A^{(2)}_{\rm T}$ [63], where $A^{(2)}_{\rm T} = S_3/(1 - F_{\rm L})$ and the $P'$ series of observables [64] with, for example, $P'_{4,5} = S_{4,5}/\sqrt{F_{\rm L}(1 - F_{\rm L})}$.

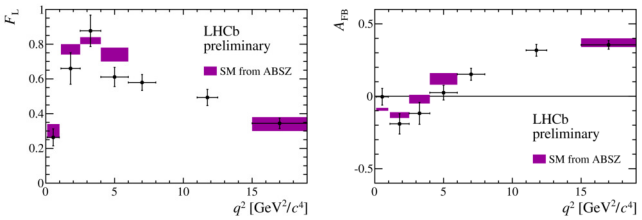


**Figure 12.** The CP-averaged observables $F_{\rm L}$ (left) and $A_{\rm FB}$ (right) in bins of $q^2$. The shaded boxes show the SM prediction taken from Ref. [71].

An unbinned maximum likelihood fit has been used to determine the CP-averaged observables $F_{\rm L}$, $A_{\rm FB}$, and $S_3$ through $S_9$. Additional observables related to the introduction of the S-wave in the $K^+\pi^-$ system are explicitely included as nuisance parameters (see Ref. [60] for more details). The data are analysed in approximately 2 GeV$^2$/c$^4$ q$^2$ bins. The SM predictions are based on the description in Ref. [62]. Light-cone sum rule predictions which are valid in the low-$q^2$ region, are combined with lattice determinations at high $q^2$ [66, 67]. The predictions are made in the regions $0.1 < q^2 < 6.0$ GeV$^2$/c$^4$ and $15.0 < q^2 < 19.0$ GeV$^2$/c$^4$. No predictions are included for the region close to the narrow $c\bar{c}$ resonances, the $J/\psi$ and $\psi(2S)$, where many of the assumptions that go into the SM predictions are thought to break down.

The results on all of the observables appear largely in agreement with the SM predictions, with the exception of the observable $S_5$. A mild tension can also be seen in the measured $A_{\rm FB}$ distribution.

We refer the reader to Ref. [60] for the full set of measured $q^2$ dependent distributions, and just show in Fig. 11 the $F_{\rm L}$ and $A_{\rm FB}$ results, including the comparison with the SM predictions.

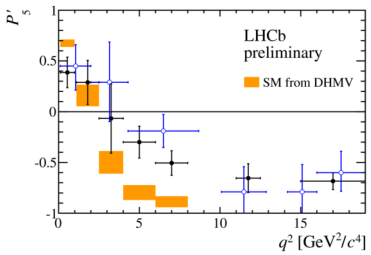


**Figure 13.** The observable $P'_5$ in bins of $q^2$. The data of the full 3.0 fb$^{-1}$ data sample are shown as black dots. The shaded boxes indicate the SM prediction taken from Ref. [68]. The blue open markers show the result of the 1.0 fb$^{-1}$ analysis from Ref. [61].

The tension in $S_5$ can also be seen in the related distribution of $P'_5 = S_5/\sqrt{F_{\rm L}(1-F_{\rm L})}$ which is shown in Fig. 13. This observable is determined by reparametrising the angular distribution accordingly. For the $P'_5$ observable, a prediction from Ref. [68] is shown. This prediction is computed in the region $0.1 < q^2 < 8.0$ GeV$^2$/c$^4$, where a local tension with the SM prediction was seen in the earlier 1.0 fb$^{-1}$ LHCb data analysis [61]. In the present analysis, a tension with the SM prediction (from Ref. [68]) at a level of $2.9\sigma$ is observed in each of the $4.0 < q^2 < 6.0$ GeV$^2$/c$^4$ and $6.0 < q^2 < 8.0$ GeV$^2$/c$^4$ bins. A naïve combination of these deviations, based on a $\chi^2$ probability with two degrees of freedom and assuming the SM predictions in the two bins are uncorrelated, yields a local tension of $3.7\sigma$. Although completely consistent with the SM predictions, the $A_{\rm FB}$ fit results are systematically $\lesssim 1\sigma$ below the SM prediction in the region with 1.0<q$^2$<6.0 GeV$^2$/c$^4$. The zero-crossing point of $A_{\rm FB}$, $q_0^2$, has been determined to be $(3.7^{+0.8}_{-1.1})$ GeV$^2/c^4$, where the uncertainty is purely statistical. The value of $q_0^2$ is in good agreement with SM predictions which are typically around 4.0 GeV$^2/c^4$, with a relative uncertainty smaller than 10% [69, 70].

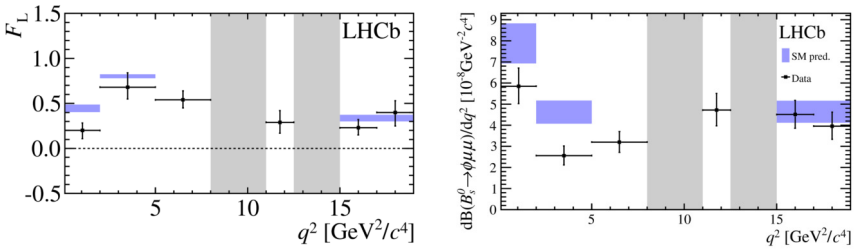


**Figure 14.** CP-averaged angular observable $F_{\rm L}$ (left) and differential branching fraction of the decay $B_s^0 \to \phi\mu^+\mu^-$ (right). Data are shown by black dots, overlaid with SM predictions [62, 71], indicated as blue shaded boxes. The vetoes excluding the charmonium resonances are indicated by grey areas.

Another $b \to s\mu^+\mu^-$ channel of interest recently studied by LHCb is the decay $B_s^0 \to \phi(\to K^+K^-)\mu^+\mu^-$ [72]. Contrary to $B^0 \to K^{*0}\mu^+\mu^-$, the above decay is self conjugate, since the final state particles provide no specific information on the $b/\bar{b}$ quark flavor. Subject to essentially the same new physics sensitivity, the $B_s^0 \to \phi\mu^+\mu^-$ channel provides good complementarity to $B^0 \to K^{*0}\mu^+\mu^-$, having an observed yield of 432 ± 24 events. With similar four-body kinematics, the full angular analysis as function of $q^2(\mu^+\mu^-)$ allows to determine four CP averages and four CP asymmetries, all of which have been determined by LHCb for the first time, using the full 3.0 fb$^{-1}$ data sample from Run 1. Physics-wise however, the observables are different from those of the $B^0 \to K^{*0}\mu^+\mu^-$, and we refer the reader to Ref. [72] for a full description of them. In particular,

there are new CP-violating asymmetries, while the $S_5$ and $A_{\rm FB}$ observables of the former channel are not accessible.

As a result of the $q^2$ dependent analysis of the eight angular observables, good consistency is found with the SM predictions for $B^0_s \to \phi\mu^+\mu^-$ [72]. However, the differential branching fraction of $(2.58^{+0.38}_{-0.31} \pm 0.08 \pm 0.19) \times 10^{-8}$ GeV$^{-2}c^4$ for $B^0_s \to \phi\mu^+\mu^-$ in the range $1 < q^2 < 6$ GeV$^2/c^4$, where precise theoretical calculations are available, is found to be more than $3\sigma$ below the SM prediction of $(4.81 \pm 0.56) \times 10^{-8}$ GeV$^2/c^4$ [62, 71]. In Fig. 14 the CP-averaged longitudinal polarization fraction $F_{\rm L}$ (left) and the differential branching fraction of $B^0_s \to \phi\mu^+\mu^-$ (right), are shown, along with the theoretical predictions.

## 8 Summary

The LHCb experiment has performed a successful physics program after completion of Run 1 at the LHC, and some recent topics on flavor physics have been selected in this article. The sensitivity to $B^0_{(s)} \to \mu^+\mu^-$ has reached the level of $10^{-10}$ and is expected to improve with integrated luminosity. A detailed comparison with the SM predictions shows general good agreement for the selected topics, although a few interesting tensions are observed, which deserve further study. Those include hints on $\tau$ lepton non-universality in $\mathcal{R}(D^*)$, a discrepancy on the $S_5$ observable in $B^0 \to K^{*0}\mu^+\mu^-$, and consistently low rates of $b \to s\mu^+\mu^-$. A precision determination of $V_{ub}$ has been achieved from a new exclusive channel, $\Lambda^0_b \to p\mu^-\bar{\nu}_\mu$, which does not support the hypothesis of $W^\pm$ right-handed currents as a possible explanation for the still standing discrepancy between inclusive and exclusive measurements of this important parameter. The Run 2 has just started at the LHC, and we hope to learn more about the above and other flavor physics issues in the near future.

## References

[1] LHCb collaboration, Alves, A.A. Jr et al., JINST 3, S088005 (2008)
[2] LHCb collaboration, Aaij et al. Int. J. Mod. Phys. A30, 1530022 (2015).
[3] T. Sjöstrand, S. Mrenna and P. Skands, Comput. Phys. Commun. 178 (2008) 852.
[4] D. J. Lange, Nucl. Inst. Meth. A462 (2001) 152.
[5] I. Belyaev et al., J. Phys. Conf. Ser. 331 (2011) 032047.
[6] Aaij et al., JINST 8, P044022 (2013).
[7] V. V. Gligorov and M. Williams, JINST 8 (2013) P02013.
[8] M. Kobayashi and T. Maskawa, Prog. Theor. Phys. 49 (1973) 652.
[9] BaBar collaboration, B. Aubert et al. Phys. Rev. Lett. 87 (2001) 091801.
Belle collaboration, K. abe et al. Phys. Rev. Lett. 87 (2001) 091802.
[10] The LHCb collaboration, R. Aaij et al., Phys. Lett. B736 (2014) 186.,
The LHCb collaboration, R. Aaij et al., Phys. Rev. D87 (2013) 112010, and
The LHCb collaboration, R. Aaij et al., Phys. Rev. Lett. 113 (2014) 211801.
[11] J. Brod and J. Zupan, JHEP 01 (2014) 051.
[12] M. Gronau and D. Wyler, Phys. Lett. B265 (1991) 172.
M. Gronau and D. London, Phys. Lett. B253 (1991) 483.
[13] D. Atwood, I. Dunietz, and A. Soni, Phys. Rev. Lett. 78 (1997) 3257.
D. Atwood, I. Dunietz, and A. Soni, Phys. Rev. D63 (2001) 036005.
[14] A. Giri, Y. Grossman, A. Soffer, and J. Zupan, Phys. Rev. D68 (2003) 054018.
[15] M. Gronau, Phys. Lett. B557 (2003) 198.

[16] Improved constraints on $\gamma$: CKM2014 update, LHCb-CONF-2014-004.
[17] BaBar collaboration, J. P. Lees et al., Phys. Rev. D87 (2013) 052015.
[18] K. Trabelsi, on behalf of the Belle collaboration at CKM2012, Cincinnati, USA, October 2012, arXiv:1301.2033.
[19] J. Charles et al. Phys. Rev. D91 (2015) 073007.
[20] The LHCb collaboration, R. Aaij et al. LHCb-PAPER-2015-020, arXiv:1505.07044.
[21] The LHCb collaboration, R. Aaij et al. Phys. Rev. D91 (2015) 112014.
[22] D. Atwood and A. Soni, Phys. Rev. D68 (2003) 033003.
[23] M. Nayak et al., Phys. Lett. B740 (2015) 1.
[24] BaBar collaboration, B. Aubert et al., Phys. Rev. D79 (2009) 072009.
Belle collaboration, I. Adachi et al., Phys. Rev. Lett. 108 (2012) 171802.
[25] The LHCb collaboration, R. Aaij et al., Phys. Rev. Lett. 115 (2015) 031601.
[26] J. Charles et al. *Current status of the Standard Model CKM fit and constraints on* $\Delta F = 2$ *New Physics*, arXiv:1501.05013.
[27] The LHCb collaboration, R. Aaij et al., Nature Physics DOI:10.1038/NPHYS3415.
[28] H.J. Rothe,*Lattice Gauge Theories: An introduction*, World Scientific Lecture Notes World Scientific, Singapore, 2012.
[29] C. A. Dominguez, Mod. Phys. Lett. A28 (2013) 1360002.
[30] Heavy Flavor Averaging Group, Y. Amhis et al., arXiv:1412.7515
http://www.slac.standord.edu/xorg/hfag/
[31] BaBar collaboration, J. P. Lees et al., Phys. Rev. D86 (2012) 092004.
P. del Amo Sanchez et al., Phys. Rev. D83 (2011) 032007.
[32] Belle collaboration, H. Ha et al., Phys. Rev. D83 (2011) 071101
A. Sibidanov et al., Phys. Rev. D88 (2013) 032005.
[33] RBC and UKQCD collaborations, J. M. Flynn et al., arXiv:1501.05373.
[34] Particle Data Group, K. A. Olive et al. Chin. Phys. C38 (2014) 090001.
[35] F. U. Bernlochner, Z. Ligeti, and S. Turczyk, Phys. Rev. D90 (2014) 094003
and other references quoted in [27].
[36] W. Detmold, C. Lehmer, and S. Meinel, arXiv:1503.01421.
[37] C. Bobeth et al., Phys. Rev. Lett. 112, 101801 (2014).
[38] RBC-UKQCD Collaborations, Witzel O, http://arXiv:org/abs/1311.0276 (2013).
HPQCD Collaboration, H. Na et al., Phys. Rev. D86, 034506 (2012).
Fermilab Lattice and MILC Collaborations, Bazakov et al., Phys. Rev. D85, 114506 (2012).
[39] C. Huang et al., Phys. Rev. D59, 011701 (1998).
S. Rai Choudhury and N. Gaur, Phys. Lett. B 451, 86-92 (1999).
[40] K. Babu and C. Kolda, Phys. Rev. Lett. 84, 228-231 (2000).
C. Bobeth et al., Phys. Rev. D64, 074014.
[41] A.J. Buras, Phys. Lett. B566, 115-119 (2003).
[42] D'Ambrosio et al., Nucl. Phys. B645, 155-187 (2002).
[43] Hoecker et al. Proc. Sci. Adv. Comput. Anal. Techn. Phys. Res. 040.
[44] S. Aoki et al., Eur. Phys. J. C74, 2890 (2014).
[45] Particle Data Group, J. Beringer et al., Phys. Rev. D86, 010001 (2012).
[46] Heavy Flavor Averaging Group, Y. Amis et al., arXiv:org/abs/1207.1158 (2012).
[47] LHCb Collaboration, R. Aaij et al., Phys. Rev. Lett. 110, 021801 (2013).
[48] The CMS and LHCb collaborations, Nature 522 (2015).

[49] R. Aaij et al. (LHCb collaboration), Phys. Rev. Lett. 115, 111803 (2015).
[50] R. Aaij et al. (LHCb collaboration), Phys. Rev. Lett. 113, 151601 (2014).
[51] M. Tanaka, Z. Phys. C67, 321. (1995).
[52] A. Matyja et al. (Belle collaboration), Phys. Rev. Lett. 99, 191807 (2007).
[53] B. Aubert et al. (BABAR collaboration), Phys. Rev. Lett. 100, 021801 (2008).
[54] A. Bozek et al. (Belle collaboration), Phys. Rev. D82, 072005 (2010).
[55] J. P. Lees et al. (BABAR collaboration), Phys. Rev. Lett. 109, 101802 (2012).
[56] J. P. Lees et al. (BABAR collaboration), Phys. Rev. D88, 072012 (2013).
[57] S. Fajfer, J. F. Kamenic, and I. Nisandzic, Phys. Rev. D85, 094025 (2012).
[58] J. A. Bailey et al. (Fermilab Lattice and MILC collaborations), Phys. Rev. Lett. 109, 071802 (2012).
[59] S. Descotes-Genon, J. Matias, and J. Virto, Phys. Rev. D88 (2013) 074002.
W. Altmannshofer and D. M. Straub, Eur. Phys. J. C73 (2013) 2646.
F. Beaujean, C. Bobeth, and D. Van Dyk, Eur. Phys. J. C74 (2014) 2897.
T. Hurth and F. Mahmoudi, JHEP 04 (2014) 097.
S. Jäger and J. Martin Camalich, JHEP 05 (2013) 043.
J. Lyon and R. Zwicky, arXiv:1406.0566.
W. Altmannshofer, S. Gori, M. Pospelov, and I. Yavin, Phys. Rev. D89 (2014) 095033.
A. Crivellin, G. D'Ambrosio, and J. Heeck, Phys. Rev. Lett. 114 (2015) 151801.
R. Gauld, F. Goertz, and U. Haisch, JHEP 01 (2014) 069.
F. Mahmoudi, S. Neshatpour, and J. Virto, Eur. Phys. J. C74 (2014) 2927.
A. Datta, M. Duraisamy, and D. Ghosh, Phys. Rev. D89 (2014) 071501.
[60] R. Aaij et al., The LHCb collaboration, LHCb-CONF-2015-002.
[61] R. Aaij et al, the LHCb collaboration, Phys. Rev. Lett. 111 (2013) 191801.
[62] W. Altmannshofer and D. M. Straub, Eur. Phys. J C75 (2015) 8, 382.
[63] F. Kruger and J. Matias, Phys. Rev. D71 (2005) 094009.
[64] S. Descotes-Genon, J. Matias, M. Ramon, and J. Virto, JHEP 01 (2013) 048.
[65] W. Altmannshofer et al., JHEP 01 (2009) 019 (2009).
[66] R. R. Horgan et al., Phys. Rev. D89 (2014) 094501.
[67] R. R. Horgan et al., PoS LATTICE 2014 (2015) 372.
[68] S. Descotes-Genon, L. Hofer, J. Matias, and J. Virto, JHEP 1412 (2014) 125.
[69] C. Bobeth et al. JHEP 01 (2012) 107.
[70] M. Beneke, T. Feldman, and D. Seidel, Eur. Phys. J. C41 (2005) 173.
[71] A. Bharucha, D.M. Straub, and R. Zwicky, arXiv:1503.05534.
[72] R. Aaij et al, the LHCb collaboration, JHEP 09 (2015), 179.